

A Brinkman penalization method for compressible flows in complex geometries

Qianlong Liu, Oleg V. Vasilyev *

Department of Mechanical Engineering, University of Colorado, 427 UCB, Boulder, CO 80309, USA

Received 15 February 2007; received in revised form 12 July 2007; accepted 25 July 2007

Available online 1 September 2007

Abstract

To simulate flows around solid obstacles of complex geometries, various immersed boundary methods had been developed. Their main advantage is the efficient implementation for stationary or moving solid boundaries of arbitrary complexity on fixed non-body conformal Cartesian grids. The Brinkman penalization method was proposed for incompressible viscous flows by penalizing the momentum equations. Its main idea is to model solid obstacles as porous media with porosity, ϕ , and viscous permeability approaching zero. It has the pronounced advantages of mathematical proof of error bound, strong convergence, and ease of numerical implementation with the volume penalization technique. In this paper, it is extended to compressible flows. The straightforward extension of penalizing momentum and energy equations using Brinkman penalization with respective normalized viscous, η , and thermal, η_T , permeabilities produces unsatisfactory results, mostly due to nonphysical wave transmissions into obstacles, resulting in considerable energy and mass losses in reflected waves. The objective of this paper is to extend the Brinkman penalization technique to compressible flows based on a physically sound mathematical model for compressible flows through porous media. In addition to penalizing momentum and energy equations, the continuity equation for *porous media* is considered inside obstacles. In this model, the penalized porous region acts as a high impedance medium, resulting in negligible wave transmissions. The asymptotic analysis reveals that the proposed Brinkman penalization technique results in the amplitude and phase errors of order $O((\eta\phi)^{1/2})$ and $O((\eta/\eta_T)^{1/4}\phi^{3/4})$, when the boundary layer within the porous media is respectively resolved or unresolved. The proposed method is tested using 1- and 2-D benchmark problems. The results of direct numerical simulation are in excellent agreement with the analytical solutions. The numerical simulations verify the accuracy and convergence rates. © 2007 Elsevier Inc. All rights reserved.

Keywords: Immersed boundary method; Brinkman penalization; Compressible flow; Porous media; Complex geometry; Compressible Navier–Stokes equations; Amplitude and phase errors; Asymptotic analysis; Theory of acoustics

* Corresponding author. Tel.: +1 303 492 4717; fax: +1 303 492 3498.

E-mail addresses: Qianlong.Liu@colorado.edu (Q. Liu), Oleg.Vasilyev@Colorado.edu (O.V. Vasilyev).

1. Introduction

Numerical simulations of viscous flows around solid obstacles of arbitrary shapes are often required for practical engineering applications. Two general techniques had been developed for the complex geometry problems. Namely, they are body-fitted grid methods [1,2] and immersed boundary techniques [3,4]. In conventional structured/unstructured body-fitted grid methods, the grids are generated to conform to the complex boundaries. Therefore, it is pretty easy to specify boundary conditions and to attain satisfactory accuracy by putting fine mesh for boundary layers, where high resolutions are required, which is critical for high Reynolds number flows. However, there are some disadvantages for these methods. The grid generation process may be very expensive: it is not an easy task to generate the grid with good quality even for simple geometries and simulations for moving boundary problems become prohibitively expensive due to grid generation and solution interpolation to the new mesh at each time step. An alternative approach, the immersed boundary methods, is to carry out simulations on non-body conformal fixed Cartesian grids and to formulate a procedure for imposing immersed boundary effects on the fluid. Its main advantage is the efficient implementation for stationary and moving solid boundaries of arbitrary complexity.

Since Peskin's immersed boundary method [5] was originally introduced to study flow patterns around heart valves, a various immersed boundary techniques had been developed. These methods had mostly been carried out for the incompressible viscous flows. In Peskin's immersed boundary method [5], incompressible flows are solved with the Navier–Stokes equations and the immersed boundary, modeled as elastic media, exerts localized forces to the fluids and modifies the momentum equations. For the solid obstacle problem, a stiff spring with a restoring force is used for the elastic media [6]. This method had been extended by Goldstein *et al.* [7] and Saiki and Biringen [8], using a feedback forcing to represent the immersed boundary effects for rigid body problems. However, these methods have some drawbacks. The methods use an explicit time-stepping scheme for the resulting stiff problems and, thus, the corresponding small computational time step severely restricts the simulations. The underlying grids are nonadaptive, making the methods inefficient for the high Reynolds number flow around solid obstacles. Finally, there is not yet any mathematical convergence proof for these methods.

A number of other immersed boundary methods had been developed for the incompressible viscous flows around complex solid boundaries. In contrast to the Peskin's immersed boundary methods using external forces to simulate the immersed boundaries, Cartesian grid methods [9–12] and ghost-cell immersed boundary method [13] directly impose the boundary conditions on the immersed boundaries. Another interesting approach is the Brinkman penalization method. This volume penalization technique was originally proposed by Arquis and Caltagirone [14]. The boundary conditions are imposed by adding the penalization terms to the momentum equations. Its main idea is to model arbitrarily complex solid obstacles as porous media with porosity ϕ and permeability approaching zero. Similar to the Peskin's immersed boundary methods, the immersed boundary exerts localized forces to the fluids and modifies the momentum equations. This method has some pronounced advantages. Boundary conditions can be enforced to a specified precision, without changing the numerical method (or grid) used to solve the equations. The main advantage of this method, compared to other penalization type methods, is that the error can be estimated rigorously in terms of the penalization parameter [15]. It can also be shown that the solution of the penalized incompressible Navier–Stokes equations strongly converges to the exact solution as the penalization parameter approaches zero [16].

By contrast, the immersed boundary methods had seldom been developed for the compressible viscous flows. The Cartesian grid method [17] was used to simulate the compressible flows around a circular cylinder and an airfoil at high Reynolds numbers by directly modifying the discretized equations near the immersed boundaries. However, the acoustic wave reflection and transmission at the interface between fluid and solid media had not been taken into account, which are critical in some applications with acoustic and shock wave propagation around solid obstacles. The Impedance Mismatch Method is another technique to model the acoustic wave propagation around solid wall boundaries using the non-body conformal cartesian grids. Originally developed by Chung [18], the Impedance Mismatch Method had only been performed for the linearized acoustic problems with steady mean flows [19–21] and has never been applied to unsteady non-uniform flow problems. Its main idea is to set a larger characteristic impedance inside the solid obstacle so that most acoustic waves are reflected by the classical theory of acoustics. For the numerical stability purpose, the non-dimensional density

is recommended to be $\rho_s = 30$ for the obstacle while $\rho_f = 1$ for fluids. This means theoretically that the reflected wave amplitude error is $1 - \frac{\rho_s - \rho_f}{\rho_s + \rho_f}$, which is approximately equal to 6.5%, and the reflected wave energy error is $1 - \left(\frac{\rho_s - \rho_f}{\rho_s + \rho_f}\right)^2$, which is approximately equal to 12.5%. These errors are not sufficiently accurate in some cases and even worse for the shock wave propagation. Another drawback of this approach is that it has no mechanism to set up the no-slip conditions and other immersed boundary conditions. Cohen et al. [22] extended this method to unsteady non-uniform flow problems. However, some serious problems for convective term handling, the stability, and accuracy of reflection for acoustic sources exist in the near vicinity of an interface.

The objective of this paper is to extend the Brinkman penalization technique to compressible flows based on a physically sound mathematical model for compressible flows through porous media. In the proposed formulation, in addition to Brinkman penalization of momentum and energy equations, the continuity equation is also modified inside the obstacle so that it is consistent with the porous media flow physics. In this model, the penalized porous region acts as a high impedance medium, resulting in negligible wave transmissions. The error bounds of the proposed compressible formulation are estimated using an asymptotic analysis of the plane acoustic wave propagation through fluid–porous media interface and verified numerically.

It should be noted that the proposed Brinkman penalization approach can be used in combination with any numerical technique as well as with body-fitted meshes. In the latter case, the penalization can be only applied to certain flow regions where geometry is modified without changing computational mesh. In addition, as pointed out by Mittal and Iaccarino [4], for high Reynolds number flows the use of the proposed approach, as well as other immersed boundary techniques, will be prohibitively expensive if no adaptive meshes are used in the vicinity of solid walls. However, if proposed or other immersed boundary techniques are implemented using adaptive mesh refinement methods, the computational cost of having additional nodes inside of the obstacle is minimal, since most of the grid points are concentrated in a thin layer close to the surface of the obstacle. The efficient use of Brinkman penalization technique for incompressible flows in the context of adaptive wavelet collocation method has been successfully demonstrated by Kevlahan and Vasilyev [23]. Another important aspect of the Brinkman penalization is that introduction of penalty terms into Navier–Stokes equations results in additional stiffness, thus requiring the use of stiffly stable solvers or implicit treatment of the penalization terms. Due to the general applicability of the proposed methodology, the numerical issues related to its implementation are not discussed in this paper. However, all the results reported in this paper were obtained using a dynamically adaptive wavelet collocation method [24–26] with Krylov time integration scheme [27]. The corresponding cost, accuracy, and implementation issues are discussed in the previous work [23] on Brinkman penalization method for incompressible flows.

The rest of the paper is organized as follows. A brief review of porous media equations for compressible flows is given in Section 2. The proposed compressible Brinkman penalization method and the corresponding accuracy and convergence, using both the theory of acoustics and asymptotic analysis, are given in Section 3. Finally, two acoustic benchmark problems are discussed in Section 4 to verify the accuracy and convergence rates of the proposed method.

2. A brief review of porous media equations

In the Brinkman penalization method [14] for incompressible flows, the solid obstacles are modeled as porous media. The governing Navier–Stokes equations for fluids and penalized Navier–Stokes equations for porous media are solved simultaneously. Thus, there is no need to specify the interface conditions directly, because they are automatically solved from the governing equations. However, appropriate interface conditions solved from the coupled governing equations are critical for satisfactory numerical solutions. Therefore, the appropriate governing equations around the boundary layer between fluids and porous media are crucial to obtain the appropriate interface conditions. To simulate compressible viscous flows around bluff bodies, a straightforward extension of the incompressible Brinkman penalization method [26] is to penalize the momentum and energy equations. However, this extension produces unsatisfactory results, mostly due to nonphysical wave transmissions into obstacles resulting in considerable energy and mass losses in reflected waves. The losses for shock wave propagation are even worse. The reason is that an inconsistent interface conditions are solved from the coupled governing equations automatically. In this section, a brief review of the physics

and the governing equations for the compressible porous media are given in order to obtain the appropriate interface conditions. For the details, we refer to books [28–30].

2.1. Some properties of porous media

Porous media consist of solid matrices with interconnected pores, which are saturated by fluids and allows fluid flows through the material. Two important length scales for the flow through permeable media are the characteristic size of pores d and the macroscopic length scale L . Two important characteristics of porous media are the porosity ϕ and the permeability K . ϕ is the volume fraction of connected pores allowing fluid flows while K is the measure of the flow conductance of the solid matrix, which is proportional to ϕd^2 .

An important flow property is the velocity. The interstitial velocity of the fluid $\mathbf{u} = (u_1, u_2, u_3)$ and the seepage or Darcy velocity $\mathbf{v} = (v_1, v_2, v_3)$ are related by the Dupuit–Forchheimer relationship [28]:

$$\mathbf{v} = \phi \mathbf{u}. \tag{1}$$

Since the porosity $\phi \ll 1$, the magnitude of \mathbf{v} is substantially smaller than that of \mathbf{u} .

2.2. Continuity equation

For the porous media, the conservation of mass can be written as

$$\frac{\partial \rho}{\partial t} = -\frac{1}{\phi} \frac{\partial}{\partial x_j} (\rho v_j), \tag{2}$$

where ρ is the interstitial fluid density, assuming that the porosity $\phi = \phi(\mathbf{x})$.

2.3. Darcy’s law, Brinkman equation and extensions

A number of momentum equations exist in the literature for the porous media. The first is the Darcy’s law [31]:

$$\mathbf{v} = -\frac{K}{\mu} \nabla p, \tag{3}$$

where μ is the dynamic viscosity and p is the intrinsic fluid pressure. In this law, the pressure gradient driving the motion balances the viscous stress gradient resisting the flow. It reveals a proportionality between the flow rate and the applied pressure gradient. In order to meet the no-slip boundary conditions requirement, by placing an additional viscous term, the Darcy’s law was extended to the well-known Brinkman equation [32,33]:

$$\nabla p = -\frac{\mu}{K} \mathbf{v} + \mu \nabla^2 \mathbf{v}, \tag{4}$$

where two viscous terms exist. The first is the usual Darcy term and the second is the Laplacian term analogous to that in the Navier–Stokes equation.

To make the momentum equation analogous to the Navier–Stokes equations, Wooding [34] extended the Darcy’s law to

$$\rho \left[\phi^{-1} \frac{\partial \mathbf{v}}{\partial t} + (\phi^{-1} \mathbf{v} \cdot \nabla)(\phi^{-1} \mathbf{v}) \right] = -\nabla p - \frac{\mu}{K} \mathbf{v}, \tag{5}$$

and Vafai and Tien [35] and Hsu and Cheng [36] extended the Brinkman equation to

$$\rho \left[\phi^{-1} \frac{\partial \mathbf{v}}{\partial t} + (\phi^{-1} \mathbf{v} \cdot \nabla)(\phi^{-1} \mathbf{v}) \right] = -\nabla p - \frac{\mu}{K} \mathbf{v} + \mu \nabla^2 \mathbf{v}. \tag{6}$$

These two extensions can be derived by the local volume-averaging method [35,30]. By incorporating the continuity equation to these two extensions, the conservative form can be written as

$$\frac{1}{\phi} \frac{\partial \rho v_i}{\partial t} = -\frac{1}{\phi} \frac{\partial}{\partial x_j} (\rho \phi^{-1} v_i v_j) - \frac{\partial p}{\partial x_i} - \frac{\mu}{K} v_i, \quad (7)$$

$$\frac{1}{\phi} \frac{\partial \rho v_i}{\partial t} = -\frac{1}{\phi} \frac{\partial}{\partial x_j} (\rho \phi^{-1} v_i v_j) - \frac{\partial p}{\partial x_i} + \mu \frac{\partial^2 v_i}{\partial x_j^2} - \frac{\mu}{K} v_i. \quad (8)$$

These momentum equations are the models for the porous media. Beck [37] pointed out that the inclusion of the convection term $(\phi^{-1} \mathbf{v} \cdot \nabla)(\phi^{-1} \mathbf{v})$ was inappropriate due to the order rising of the spatial derivatives and inconsistency with the slip boundary condition. Nield and Bejan [28] suggested to drop it in numerical work. The equations suggest that momentum decays in the order of $\exp[-(\phi/K)t]$ and even dropping the coefficients ϕ^{-1} of the left hand side, the momentum decays sufficiently fast. Thus, modification of the left hand side does not change the solutions much. In the actual governing equations of the proposed model, the momentum equation is further simplified to make it analogous to the compressible Navier–Stokes equation with additional Brinkman penalization term, thus resulting in straightforward implementation. This simplification is possible since the penalization term results in significant damping of the momentum inside of the porous media, while satisfying consistent no-slip boundary at the interface.

2.4. Energy equation

Finally, the energy equation can be written as

$$\frac{\partial e}{\partial t} = -\frac{\partial}{\partial x_j} [(e+p)v_j] + \frac{\partial}{\partial x_j} \left(k \frac{\partial T}{\partial x_j} \right) - \frac{h}{\phi} (T - T_0), \quad (9)$$

where heat transfer between solid and fluid are allowed for thermal non-equilibrium, e is the total energy, h is a heat transfer coefficient, and T_0 is the solid temperature.

3. Brinkman penalization method for compressible flows

Before considering the compressible flows, a brief review of the Brinkman penalization method for the incompressible flows is given. Then, it is extended to compressible flows, by combining the Navier–Stokes equations and the compressible porous media equations and making the resulting momentum equations analogous to those in the incompressible Brinkman penalization method. Finally in this section, the corresponding error bounds are analyzed using the theory of acoustics and asymptotic analysis.

3.1. Brinkman penalization method for incompressible flows

A viscous incompressible fluid is governed by the Navier–Stokes equations

$$\frac{\partial \mathbf{u}}{\partial t} + \mathbf{u} \cdot \nabla \mathbf{u} + \nabla P = \nu \Delta \mathbf{u}, \quad (10)$$

For the direct numerical simulation (DNS), consider a viscous incompressible flows around a set of obstacles O_i . The flows are simulated numerically in a rectangular domain $\Omega = [L_1, L_2] \times [M_1, M_2]$ containing all the obstacles O_i . On the surface of the obstacles the velocity must satisfy the no-slip condition,

$$\mathbf{u} = \mathbf{U}_o \quad \text{on } \partial O_i, \quad \forall i, \quad (11)$$

where \mathbf{U}_o is the velocity of the obstacle.

To model the effect of the no-slip boundary conditions on the obstacles O_i without explicitly imposing (11), we follow Angot et al. [15] by replacing (10) and (11) by the following set of L^2 -penalized equations

$$\frac{\partial \mathbf{u}}{\partial t} + \mathbf{u} \cdot \nabla \mathbf{u} + \nabla P = \nu \Delta \mathbf{u} - \frac{1}{\eta} \chi(\mathbf{x}, t) (\mathbf{u} - \mathbf{U}_o), \quad (12)$$

Note that Eq. (12) are valid in the entire domain Ω : the last term on the right hand side of (12) is a volume penalization of the flow inside the obstacle. Here, $0 < \eta \ll 1$ is a penalization coefficient and χ denotes the characteristic (or mask) function

$$\chi(\mathbf{x}, t) = \begin{cases} 1 & \text{if } \mathbf{x} \in O_i, \\ 0 & \text{otherwise.} \end{cases} \tag{13}$$

3.2. Brinkman penalization method for compressible flows

The governing full compressible Navier–Stokes equations are as follows:

$$\frac{\partial \rho}{\partial t} = -\frac{\partial m_j}{\partial x_j}, \tag{14}$$

$$\frac{\partial m_i}{\partial t} = -\frac{\partial m_i u_j}{\partial x_j} - \frac{\partial p}{\partial x_i} + \frac{\partial \tau_{ij}}{\partial x_j}, \tag{15}$$

$$\frac{\partial e}{\partial t} = -\frac{\partial}{\partial x_j} [(e + p)u_j] + \frac{\partial}{\partial x_j} (u_i \tau_{ij}) + \frac{\partial}{\partial x_j} \left(k \frac{\partial T}{\partial x_j} \right), \tag{16}$$

where

$$p = \rho RT,$$

$$\tau_{ij} = \mu \left(\frac{\partial u_i}{\partial x_j} + \frac{\partial u_j}{\partial x_i} - \frac{2}{3} \frac{\partial u_k}{\partial x_k} \delta_{ij} \right),$$

$$e = \frac{1}{2} \rho u_i u_i + \frac{p}{\gamma - 1},$$

where ρ is the density of the fluid (gas), $m_j = \rho u_j$ is the mass flux, p is the pressure, τ_{ij} is the shear stress tensor, μ is the coefficient of dynamic viscosity of the fluid, which is temperature dependent, e is the total energy, k is the thermal conductivity which is temperature dependent, T is the absolute temperature, $R = (\gamma - 1)c_v$ is the gas constant, and $\gamma = \frac{c_p}{c_v}$.

On the surface of the obstacles the velocity must satisfy the no-slip condition, while temperature of the object is assumed constant

$$\left. \begin{aligned} \mathbf{u} &= \mathbf{U}_o \\ T &= T_o \end{aligned} \right\} \text{ on } \partial O_i, \forall i, \tag{17}$$

where \mathbf{U}_o and T_o are respectively, the velocity and the temperature of the obstacle. To specify the no-slip boundary conditions and temperature on the obstacles O_i without explicitly imposing (17), we can simply follow the Angot et al. [15] by adding penalty terms into momentum and energy equations. However, this straightforward extension produces unsatisfactory results, mostly due to nonphysical wave transmissions into solid obstacles, resulting in considerable energy and mass losses in reflected waves. By incorporating the two sets of Navier–Stokes equations and porous media equations and making the momentum equation analogous to that in the incompressible Brinkman penalization method, the non-dimensional Brinkman penalization method for the compressible flows becomes:

$$\frac{\partial \rho}{\partial t} = -\left[1 + \left(\frac{1}{\phi} - 1 \right) \chi \right] \frac{\partial m_j}{\partial x_j}, \tag{18}$$

$$\frac{\partial m_i}{\partial t} = -\frac{\partial}{\partial x_j} (m_i u_j) - \frac{\partial p}{\partial x_i} + \frac{1}{Re_a} \frac{\partial \tau_{ij}}{\partial x_j} - \frac{\chi}{\eta} (u_i - U_{oi}), \tag{19}$$

$$\frac{\partial e}{\partial t} = -\frac{\partial}{\partial x_j} [(e + p)u_j] + \frac{1}{Re_a} \frac{\partial}{\partial x_j} (u_i \tau_{ij}) + \frac{1}{Re_a Pr (\gamma - 1)} \frac{\partial}{\partial x_j} \left(\mu \frac{\partial T}{\partial x_j} \right) - \frac{\chi}{\eta_T} (T - T_o), \tag{20}$$

where

$$\begin{aligned}
 p &= \rho T / \gamma, \\
 \tau_{ij} &= \mu \left(\frac{\partial u_i}{\partial x_j} + \frac{\partial u_j}{\partial x_i} - \frac{2}{3} \frac{\partial u_k}{\partial x_k} \delta_{ij} \right), \\
 e &= \frac{1}{2} \rho u_i u_i + \frac{p}{\gamma - 1},
 \end{aligned}$$

ϕ is the porosity, $\eta = \alpha\phi$ is a normalized viscous permeability, $\eta_T = \alpha_T\phi$ is a normalized thermal permeability, $Re_a = \frac{\rho_0 c_0 L}{\mu_0}$ is the acoustic Reynolds number, $Pr = \frac{\mu_0 c_p}{k}$ is the Prandtl number, and U_o and T_o are the obstacle’s normalized velocity and temperature. Note that in the subsequent analysis the following inequality are assumed: $0 < \phi \ll 1$, $0 < \eta \ll 1$, and $0 < \eta_T \ll 1$. The variables of velocity, length, time, energy, density, pressure, viscosity, thermal conductivity, and temperature are respectively non-dimensionalized by the reference speed of sound c_0 , characteristic length L , L/c_0 , c_0^2 , the reference density ρ_0 , $\rho_0 c_0^2$, the reference viscosity μ_0 , $\mu_0 c_p$, and the reference temperature T_0 . Note that the pressure is not non-dimensionalized by the reference pressure $p_0 = \rho_0 R T_0$. Also note that Eqs. (18)–(20) are valid in the entire domain Ω : the last term on the right hand side of Eqs. (19) and (20) is a volume penalization of the flow and temperature inside the obstacle.

The compressible Brinkman penalized Navier–Stokes Eqs. (18)–(20) can be used for general compressible flow simulations. Due to the difficulty of obtaining exact error bounds for general case, in the following Sections 3.3 and 3.4 the amplitude and phase error analysis is performed for the case of acoustic wave propagation in the small amplitude limit and the error bounds are established. Due to physical consistency of the proposed methodology and independence of the asymptotic expansion in the porous media region on the wave amplitude, as explained in Section 3.4, the error estimates are valid for the general subsonic flows. However, the error analysis presented in this paper is not valid for the case of incident shock wave. The extension of the analysis for the Euler equations with shock waves and the use of the Brinkman penalization technique with hyperbolic solvers is currently under investigation.

3.3. Amplitude error estimates by acoustics theory

In this section, the amplitude error are estimated by the classical theory of acoustics [38] from the physical viewpoint. Consider the plane wave reflection and transmission at the interface between two different media. The 1-D problem of wave propagation in fluid-porous media is modeled in a sudden change in cross-sectional area and is sketched in Fig. 1. From the acoustics theory, the reflection coefficient \mathcal{R} can be written as

$$\mathcal{R} \equiv \frac{p^{\text{in}}}{p^{\text{ref}}} = \frac{Z_2 - Z_1}{Z_2 + Z_1}, \tag{21}$$

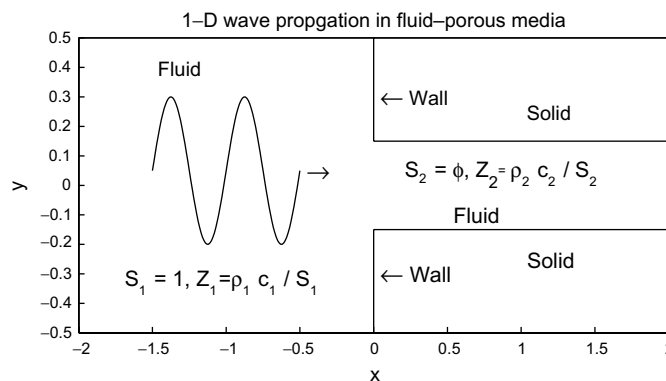


Fig. 1. 1-D model of wave propagation in fluid-porous media.

where p^{in} is the incident acoustic pressure, p^{ref} is the reflected acoustic pressure, and Z_1 and Z_2 are the acoustic impedance for the two media. The acoustic impedance at a given surface is the ratio of the surface-averaged acoustic pressure to the fluid volume velocity:

$$Z = \rho c/S, \tag{22}$$

where ρ is the density, c is the speed of sound, and S is the cross-sectional area.

The reflection coefficient formula suggests that the only way to make most parts of waves reflected from the obstacles is to set the obstacle’s acoustic impedance sufficiently large. This is the basis for the Impedance Mismatch Method [18] which uses the relatively low impedance ratio of value 30. For the proposed Brinkman penalization method, suppose that porous media consist of a distribution of parallel tubes inside the solid matrix. The corresponding reflection coefficient can be written as

$$\mathcal{R} = \frac{1 - \phi}{1 + \phi} \approx 1 - 2\phi, \tag{23}$$

where the same density and speed of sound for both media are assumed. The result of the amplitude error of order $O(\phi)$ for the reflected wave is consistent with the results from the following asymptotic analysis. Thus, for a sudden change in cross-sectional area between fluids and porous media, the porous media act as a high impedance medium with $Z = \rho c/\phi$, resulting in negligible wave transmissions.

3.3.1. Speed of sound in porous media

This subsection is used to verify the assumption that the speeds of sound in both media are same in the limit of small porosity. For simplicity, we consider the dimensional Euler equations for the conservative variables:

$$\frac{\partial \mathbf{u}}{\partial t} + \mathbf{A} \frac{\partial \mathbf{u}}{\partial x} = 0, \tag{24}$$

where $\mathbf{u} = \{\rho \ \rho u \ e\}^T$ is the vector of the conservative variables and the Jacobian matrix can be written as

$$\mathbf{A} = \begin{bmatrix} 0 & \phi^{-1} & 0 \\ \frac{\gamma-3}{2}u^2 & (3-\gamma)u & \gamma-1 \\ -\gamma u e \rho^{-1} + (\gamma-1)u^3 & \gamma e \rho^{-1} - \frac{3}{2}(\gamma-1)u^2 & \gamma u \end{bmatrix},$$

where

$$e = \frac{1}{2}\rho u^2 + \frac{p}{\gamma-1}.$$

Note that the case $\phi = 1$ is for the fluid region while other cases are for the porous media. For the details of deriving this Jacobian matrix, we refer the reader to Chapter 2 in the classical Laney’s computational gasdynamics textbook [39]. Then term $e \rho^{-1}$ can be simplified for convenience as follows

$$\frac{e}{\rho} = \frac{1}{2}u^2 + \frac{p}{(\gamma-1)\rho} = \frac{1}{2}u^2 + \frac{c^2}{\gamma(\gamma-1)},$$

where c is defined as $(\gamma p/\rho)^{1/2}$. Note that at this point c is only a notation and is not associated with the speed of sound.

To find the speeds of sound for both regions, the eigenvalues of the Jacobian matrix \mathbf{A} need be first found by solving the characteristic equation

$$|\mathbf{A} - \lambda \mathbf{I}| = 0, \tag{25}$$

which can be expanded to the depressed (or standard) cubic equation

$$-(\lambda - u)^3 + \left[c^2 + \frac{u^2}{2}(\phi^{-1} - 1)(\gamma - 3) \right] (\lambda - u) - c^2 u (\phi^{-1} - 1) + \frac{u^3}{2}(\phi^{-1} - 1)(\gamma - 1) = 0.$$

Setting $\phi = 1$ for the fluid region yields three eigenvalues of u , $u - c$, and $u + c$. This implies the speed of sound in the fluid region is c . For the porous media part, the eigenvalues are complicated, although three

analytical roots can be found by the Cardano’s method. However, due to the strong damping effects for the porous media region as indicated in Section 3.4 $u \sim O(\alpha\phi)$, where $0 < \alpha, \phi \ll 1$. Thus, ignoring the higher order terms in the analytical solutions, three eigenvalues can be found to be u , $u - c$, and $u + c$, which implies that the low porosity limit the speed of sound in the porous media is also c . Therefore, the speeds of sound are same inside and outside of the porous media.

3.4. Amplitude and phase errors by asymptotic analysis

In this section, the amplitude and phase errors are estimated by the asymptotic analysis from the rigorous mathematical viewpoint. Consider the incident waves with amplitude of order ϵ . The 1-D problem of wave propagation in fluid-porous media is sketched in Fig. 2. Note that the leading term asymptotic analysis for the porous media region reported in this section assumes only low porosity and permeability limits and, thus, can be used even for the large amplitude incident waves, i.e. $\epsilon = O(1)$. Therefore, error estimates reported in this section are valid for general subsonic flows. However, in order to obtain analytical solution in the entire domain the small amplitude of the wave is explicitly assumed in the fluid region.

3.4.1. Asymptotic analysis for the fluid region

For the fluid region, the variables can be written as, keeping only the leading perturbation terms,

$$\rho_f(x, t) = 1 + \epsilon\rho'_f + \dots, \quad u_f(x, t) = \epsilon u'_f + \dots, \tag{26}$$

$$p_f(x, t) = \frac{1}{\gamma} + \epsilon p'_f + \dots, \quad T_f(x, t) = 1 + \epsilon T'_f + \dots \tag{27}$$

where $\epsilon \ll 1$. By substituting them into Eqs. (18)–(20) and the equation of state, the leading terms result in the classical acoustic wave equations

$$\frac{\partial^2 p'_f}{\partial t^2} = \frac{\partial^2 p'_f}{\partial x^2}, \quad \frac{\partial^2 u'_f}{\partial t^2} = \frac{\partial^2 u'_f}{\partial x^2}, \tag{28}$$

and the isentropic relation

$$\rho'_f = p'_f, \quad T'_f = (\gamma - 1)p'_f. \tag{29}$$

Thus, the classical acoustics theory [38] for plane wave propagation can be easily used. Note that the relation $\rho'_f = p'_f$ results in the fact that the temperature perturbation is of same order of the ρ and p perturbations in the fluid region.

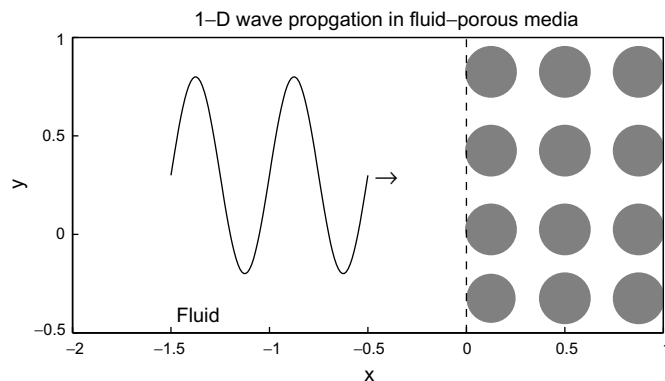


Fig. 2. 1-D wave propagation in fluid-porous media.

3.4.2. Asymptotic analysis for porous media region

For the porous media region, the variables can be written as, keeping only the leading perturbation terms,

$$\rho_p(x, t) = 1 + \epsilon \rho'_p + \dots, \quad u_p(x, t) = \epsilon \eta u'_p + \dots, \tag{30}$$

$$p_p(x, t) = \frac{1}{\gamma} + \epsilon p'_p + \dots, \quad T_p(x, t) = 1 + \epsilon \eta_T T'_p + \dots, \tag{31}$$

where the leading perturbation terms of u_p and T_p are different from their counterparts in the fluid region, due to the strong Brinkman damping terms in the momentum and energy equations. Substituting them into Eqs. (18)–(20) and the equation of state yields the relations

$$\rho'_p = \gamma p'_p, \quad \frac{\partial p'_p}{\partial t} + (\gamma - 1) T'_p = 0, \tag{32}$$

and the partial differential equations:

$$\frac{\partial \rho'_p}{\partial t} + \alpha \frac{\partial u_p}{\partial x} = 0, \quad \frac{\partial p_p}{\partial x} + u'_p = 0, \tag{33}$$

where $\alpha = \eta/\phi$. Eq. (33) can be further reduced to

$$\frac{\partial p'_p}{\partial t} = \frac{\alpha}{\gamma} \frac{\partial^2 p'_p}{\partial x^2}, \quad \frac{\partial u'_p}{\partial t} = \frac{\alpha}{\gamma} \frac{\partial^2 u'_p}{\partial x^2}. \tag{34}$$

Thus, different from the fluid region governing by the wave equations, the porous media are governed by the diffusion equations. As a result, the complex function method for solving problems with harmonic oscillating boundary conditions problem [40] can be applied easily. Note that the relation $\rho'_p = \gamma p'_p$ results from the fact that the temperature perturbation is relatively very small, compared with the density and pressure perturbations.

3.4.3. Asymptotic analysis for the boundary layer

The above asymptotic analysis is valid for the fluid and porous media regions away from the porous media interface, because the length and magnitude scales of the perturbations are valid in the two regions. However, it is not valid in the immediate vicinity of the interface inside of the porous media. This fact is implied by the conflicting relations between the perturbation of ρ and p in Eqs. (29) and (32) at the interface. This conflict results from the different length and magnitude scales for the perturbation of T in Eqs. (27) and (31). Thus, to get correct results, a boundary layer inside the porous media is needed to consider in order to match the two solutions in the fluid and porous media regions. Note that for the fluid region, the perturbations of ρ , p , and T have the same magnitude scale of $O(\epsilon)$. Since the solutions in the boundary layer match those in the fluid region at their interface, these three perturbations have the same magnitude scale of $O(\epsilon)$ in both regions. For the boundary layer, the variables can be written as, keeping only the leading perturbation terms,

$$\rho_b(x, t) = 1 + \epsilon \rho'_b + \dots, \quad u_b(x, t) = \epsilon \eta u'_b + \dots, \tag{35}$$

$$p_b(x, t) = \frac{1}{\gamma} + \epsilon p'_b + \dots, \quad T_b(x, t) = 1 + \epsilon T'_b + \dots. \tag{36}$$

Substituting them into Eqs. (18)–(20) and the equation of state for the porous media results in the governing equations for the boundary layer

$$\frac{\partial \rho'_b}{\partial t} = -\alpha \frac{\partial u'_b}{\partial x}, \tag{37}$$

$$\frac{\partial p'_b}{\partial x} = -u'_b, \tag{38}$$

$$\frac{\partial p'_b}{\partial t} = -\frac{1}{\eta_T} (\gamma - 1) T'_b, \tag{39}$$

$$\gamma p'_b = \rho'_b + T'_b. \tag{40}$$

Since ρ'_b and p'_b are of same order, the time derivatives $\frac{\partial \rho'_b}{\partial t}$ and $\frac{\partial p'_b}{\partial t}$ are of same order. That means that $\alpha \frac{\partial^2 p'_b}{\partial x^2}$ and $\frac{1}{\eta_T}(\gamma - 1)T'_b$ are of same order, which suggests that the thickness of the boundary layer is $O(\delta)$, where $\delta = (\alpha\eta_T)^{1/2}$. This thickness is also the length scale for ρ'_b and T'_b . Since ρ'_b and u'_b couple through Eq. (37), they share the same length scale. Due the small thickness of the boundary layer, Eq. (38) suggests that the length scale for p'_b is $O(1)$.

Eqs. (37)–(40) is the approximate governing equations for the boundary layer. However, the very thin boundary layer with thickness of $O((\alpha\eta_T)^{1/2})$ may become a very strict constrain for the numerical simulations. Note that to resolve the boundary layer, around 10 mesh points need to put there, which makes the space step size to be around $O((\alpha\eta_T)^{1/2}/10)$. This size is extremely small for small α and η_T values, which are needed to satisfy the imposed immersed boundary conditions. However, the boundary layer is not so strong, since ρ'_b change only from p'_f to $\gamma p'_b$. Thus, in order to get accurate numerical results, it is unnecessary to resolve the boundary layer. On the other hand, the convergence rates for the resolved and unresolved cases are different and will be shown to be $O(\alpha^{1/2}\phi)$ and $O((\eta/\eta_T)^{1/4}\phi^{3/4})$. Thus, both cases give accurate numerical results. These rates can be viewed as estimates for the numerical error bounds and, thus, $\alpha^{1/2}\phi$ or $(\eta/\eta_T)^{1/4}\phi^{3/4}$ should be sufficiently small to guarantee the accuracy of the numerical solution. In addition, in order to satisfy the no-slip and isothermal boundary conditions the damping inside of the porous media should be fast enough not to interfere with the external flow time scales and, thus, the magnitude of $\alpha\phi$ and $\alpha_T\phi$ should be small. In particular for turbulent flows at high Reynolds numbers with a wide range of time scales, these two damping coefficients need to be sufficiently small to ensure that the time scales associated with penalty terms are smaller than those of the energetic part of the turbulent flows. These conditions set the guidelines for the selection of the three penalty parameters. In Section 4 two special cases are chosen to numerically verify these convergence rates. The first is the case with $\alpha = 10^{-2}$, $\alpha_T = 10^{-2}$, and the convergence rate of $O(\phi)$ and $O(\phi^{3/4})$, respectively. The second is the case with $\alpha = \phi$, $\alpha_T = (\gamma - 1)$, and the convergence rate of $O(\phi^{3/2})$ and $O(\phi)$, respectively.

3.4.4. Accuracy and convergence rates for the resolved boundary layer

If the boundary layer is resolved, the governing Eqs. (37)–(40) can be reduced to the governing equation

$$\frac{\partial^2 f}{\partial t^2} = -\frac{1}{\eta_T}(\gamma - 1)\left(\gamma \frac{\partial f}{\partial t} - \alpha \frac{\partial^2 f}{\partial x^2}\right), \tag{41}$$

where f is the variable ρ'_b , p'_b , T'_b , or u'_b . This is a wave equation with strong damping effects, which the numerical simulations use to solve the boundary layer.

The solutions for the fluid region and the boundary layer can be obtained by matching them at the interface between the fluid and the boundary layer. Since any smooth wave can be decomposed into the sum of harmonic waves, without loss of generality, an incident acoustic harmonic wave with normalized amplitude from the fluid region with the interface at $x = 0$ are considered. The reflected wave has some amplitude and phase errors such that, from the classical acoustics theory [38] for the plane wave propagation, the superposition of the incident and reflected waves at the interface is of the form

$$u'_f(x = 0, t) = [1 - A \exp(i\theta)] \exp(i\omega t), \tag{42}$$

$$p'_f(x = 0, t) = [1 + A \exp(i\theta)] \exp(i\omega t). \tag{43}$$

It is assumed that

$$A = 1 + \alpha\phi A_1, \quad \theta = \alpha\phi\theta_1, \tag{44}$$

where the amplitude error $\alpha\phi A_1 \ll 1$ and the phase error $\alpha\phi\theta_1 \ll 1$, which will be verified. In the absence of shock waves the velocity and pressure are continuous in the entire domain. Thus, at the interface $x = 0$, $u_f = u_b$ and $p_f = p_b$, i.e., $u'_f = \alpha\phi u'_b$ and $p'_f = p'_b$, and the interface conditions for the leading order porous media solution at $x = 0$ are of the form

$$u'_b(x = 0, t) \approx -(A_1 + i\theta_1) \exp(i\omega t), \tag{45}$$

$$p'_b(x = 0, t) \approx 2 \exp(i\omega t). \tag{46}$$

The other boundary conditions are that perturbation velocity and pressure are finite at $x \rightarrow \infty$.

For this problem with harmonic oscillating boundary conditions, the complex function method [40] can be used to solve Eq. (41) by seeking f in the form

$$f(x, t) = g(x) \exp(i\omega t). \tag{47}$$

Plugging this into the governing equation yields

$$\frac{d^2 g}{dx^2} = \left[i \frac{\omega \gamma}{\alpha} - \frac{\omega^2 \eta_T}{\alpha(\gamma - 1)} \right] g, \tag{48}$$

for which the general solution can be written as

$$g(x) = C \exp(\lambda_1 x) + D \exp(\lambda_2 x), \tag{49}$$

where

$$\lambda_{1,2} = \pm \left[i \frac{\omega \gamma}{\alpha} - \frac{\omega^2 \eta_T}{\alpha(\gamma - 1)} \right]^{1/2} = \pm \frac{1 + i}{\sqrt{2}} \left(\frac{\gamma \omega}{\alpha} \right)^{1/2} \left[1 + \frac{\omega \eta_T}{\gamma(\gamma - 1)} i \right]^{\frac{1}{2}}. \tag{50}$$

For sufficiently small $\eta_T \ll \gamma(\gamma - 1)/\omega$ Eq. (50) can be simplified

$$\lambda_{1,2} \approx \pm \frac{1 + i}{\sqrt{2}} \left(\frac{\gamma \omega}{\alpha} \right)^{1/2} \left[1 + \frac{1}{2} \frac{\omega \eta_T}{\gamma(\gamma - 1)} i \right]. \tag{51}$$

Keeping only the leading term yields

$$\lambda_{1,2} \approx \pm (1 + i) \left(\frac{\gamma \omega}{2\alpha} \right)^{1/2}. \tag{52}$$

The general solution can be used to find the solutions for u'_b and p'_b after incorporating the boundary conditions.

The corresponding solutions for the resolved boundary layer become

$$u'_b(x, t) = -(A_1 + i\theta_1) \exp \left[-(1 + i) \left(\frac{\gamma \omega}{2\alpha} \right)^{1/2} x + i\omega t \right], \tag{53}$$

$$p'_b(x, t) = 2 \exp \left[-(1 + i) \left(\frac{\gamma \omega}{2\alpha} \right)^{1/2} x + i\omega t \right]. \tag{54}$$

By substituting the solutions to Eq. (38), the following relations are obtained

$$A_1 = \theta_1 = -(2\gamma\omega/\alpha)^{1/2}, \tag{55}$$

and thus, the amplitude and phase errors are as follows

$$\alpha\phi A_1 = \alpha\phi\theta_1 = -(2\gamma\omega\alpha)^{1/2} \phi = -(2\gamma\omega)^{1/2} (\eta\phi)^{1/2}, \tag{56}$$

from which $\alpha\phi A_1 = \alpha\phi\theta_1 \ll 1$ is verified.

Therefore, the amplitude and phase errors are of $O(\alpha^{1/2}\phi)$. This can be viewed as an estimate for the numerical error bound and, thus, the magnitude of the porosity ϕ should be sufficiently small to guarantee the accuracy of the numerical solution.

3.4.5. Accuracy and convergence rates for the unresolved boundary layer

If the boundary layer is unresolved, Eqs. (37)–(40) no longer accurately describe the numerical approximation. Instead, the terms containing spatial derivatives of the unresolved variables need to be adjusted to correspond to the outer layer solution. In order to derive governing equations consistent with the numerical approximation, the spatial variable needs to be rescaled as $x = \delta X$, where the boundary thickness $\delta = (\alpha\eta_T)^{1/2}$. This yields

$$\frac{\partial \rho'_b}{\partial t} = -\alpha \frac{1}{\delta} \frac{\partial u'_b}{\partial X}, \tag{57}$$

$$\frac{1}{\delta} \frac{\partial p'_b}{\partial X} = -u'_b, \tag{58}$$

$$\frac{\partial p'_b}{\partial t} = -\frac{1}{\eta_T}(\gamma - 1)T'_b, \tag{59}$$

$$\gamma p'_b = \rho'_b + T'_b. \tag{60}$$

If the boundary layer for u'_b is resolved, $\frac{\partial u'_b}{\partial X} = O(1)$, which would make $\frac{\partial u'_b}{\partial x} = O(\delta^{-1})$ inside boundary layer. In contrast for the unresolved boundary layer, $\frac{\partial u'_b}{\partial x} = O(1)$, which makes $\frac{\partial u'_b}{\partial X} = O(\delta)$. However, due to the fact that the boundary layer is next to the porous media interface, the solution inside of the porous media needs to be matched with the interface boundary conditions, which would make $\frac{\partial u'_b}{\partial X} = O(1)$. Thus, in order to mimic the numerical approximation of $\frac{\partial u'_b}{\partial x}$ for the unresolved boundary layer case, $\frac{1}{\delta} \frac{\partial u'_b}{\partial X}$ needs to be replaced by $\frac{\partial u'_b}{\partial X}$, which would lead to the following set of equations

$$\frac{\partial \rho'_b}{\partial t} = -\alpha \frac{\partial u'_b}{\partial X}, \tag{61}$$

$$\frac{1}{\delta} \frac{\partial p'_b}{\partial X} = -u'_b, \tag{62}$$

$$\frac{\partial p'_b}{\partial t} = -\frac{1}{\eta_T}(\gamma - 1)T'_b, \tag{63}$$

$$\gamma p'_b = \rho'_b + T'_b, \tag{64}$$

which can be reduced to the governing equation

$$\frac{\partial^2 f}{\partial t^2} = -\frac{1}{\eta_T}(\gamma - 1) \left[\gamma \frac{\partial f}{\partial t} - \left(\frac{\alpha}{\eta_T} \right)^{1/2} \frac{\partial^2 f}{\partial X^2} \right] \tag{65}$$

where f is the variable ρ'_b, p'_b, T'_b , or u'_b . This is a wave equation with strong damping effects, which the numerical simulations use to solve the unresolved boundary layer.

The solutions for the fluid region and the boundary layer can be obtained by the similar matching procedure in Section 3.4.4. For the same harmonic incident wave, the boundary conditions at $X = 0$ are of the form, only keeping the leading terms,

$$u'_b(X = 0, t) \approx -(A_1 + i\theta_1) \exp(i\omega t), \tag{66}$$

$$p'_b(X = 0, t) \approx 2 \exp(i\omega t). \tag{67}$$

The other boundary conditions are that perturbation velocity and pressure are finite at $X \rightarrow \infty$. For this problem with harmonic oscillating boundary conditions, the complex function method can be applied to solve Eq. (65). The general solution can be written as

$$f(X, t) = C \exp(\lambda_1 X + i\omega t) + D \exp(\lambda_2 X + i\omega t), \tag{68}$$

where

$$\lambda_{1,2} = \pm(1 + i) \left(\frac{\gamma\omega}{2} \right)^{1/2} \left(\frac{\eta_T}{\alpha} \right)^{1/4} \tag{69}$$

for sufficiently small $\eta_T \ll \gamma(\gamma - 1)/\omega$. This general solution can be used to find the solutions for u'_b and p'_b after incorporating the boundary conditions.

The corresponding solutions for the unresolved boundary layer become

$$u'_b(X, t) = -(A_1 + i\theta_1) \exp \left[-(1 + i) \left(\frac{\gamma\omega}{2} \right)^{1/2} \left(\frac{\eta_T}{\alpha} \right)^{1/4} X + i\omega t \right], \tag{70}$$

$$p'_b(X, t) = 2 \exp \left[-(1 + i) \left(\frac{\gamma\omega}{2} \right)^{1/2} \left(\frac{\eta_T}{\alpha} \right)^{1/4} X + i\omega t \right]. \tag{71}$$

By substituting the solutions to Eq. (62), the following relations are obtained

$$A_1 = \theta_1 = -(2\gamma\omega)^{1/2} (\alpha^3 \eta_T)^{-1/4}, \tag{72}$$

and thus, the amplitude and phase errors are as follows

$$\alpha\phi A_1 = \alpha\phi\theta_1 = -(2\gamma\omega)^{1/2}(\alpha/\eta_T)^{1/4}\phi = -(2\gamma\omega)^{1/2}(\eta/\eta_T)^{1/4}\phi^{3/4}, \tag{73}$$

from which $\alpha\phi A_1 = \alpha\phi\theta_1 \ll 1$ is verified.

Therefore, the amplitude and phase errors are of $O((\eta/\eta_T)^{1/4}\phi^{3/4})$. This can be viewed as an estimate for the numerical error bound when the boundary layer is not properly resolved. Once again, the porosity ϕ can be set to a small value to guarantee the accuracy of the numerical solution.

3.4.6. Solutions in porous media

In this section a solution in porous media outside of the boundary layer is discussed. For the unresolved boundary case, the solutions in Eqs. (70) and (71) for the boundary layer can be rewritten in terms of x as

$$u'_b(x, t) = -(A_1 + i\theta_1) \exp \left[-(1 + i) \left(\frac{\gamma\omega}{2} \right)^{1/2} (\alpha^3 \eta_T)^{-1/4} x + i\omega t \right], \tag{74}$$

$$p'_b(x, t) = 2 \exp \left[-(1 + i) \left(\frac{\gamma\omega}{2} \right)^{1/2} (\alpha^3 \eta_T)^{-1/4} x + i\omega t \right]. \tag{75}$$

The solution for the porous media can be obtained by matching it with the solution for the boundary layer at their interface. Since the length scale of the boundary layer is of $O(\delta)$, where $\delta = (\alpha\eta_T)^{1/2} \ll 1$, the solution at the interface can be obtained, by setting $x = \beta\delta$, where β is a constant related to numerical discretization. This yields

$$u'_b(x, t)|_{x=\beta\delta} = -(A_1 + i\theta_1) \exp \left[-(1 + i)\beta \left(\frac{\gamma^2\omega^2\eta_T\phi}{4\eta} \right)^{1/4} + i\omega t \right], \tag{76}$$

$$p'_b(x, t)|_{x=\beta\delta} = 2 \exp \left[-(1 + i)\beta \left(\frac{\gamma^2\omega^2\eta_T\phi}{4\eta} \right)^{1/4} + i\omega t \right]. \tag{77}$$

Since $\phi \ll 1$ and the variables match at the interface, the boundary conditions for the porous media can be written as

$$u'_p(x, t)|_{x=0} = -(A_1 + i\theta_1) \exp(i\omega t), \tag{78}$$

$$p'_p(x, t)|_{x=0} = 2 \exp(i\omega t). \tag{79}$$

The other boundary conditions are that perturbation velocity and pressure are finite at $x \rightarrow \infty$. For this problem with harmonic oscillating boundary conditions, the solution for the porous media is given by Eqs. (53) and (54) with A_1 and θ_1 obtained from Eq. (72) for the unresolved boundary layer case. The same procedure give the same formula for the resolved boundary layer case. However, A_1 and θ_1 come from Eq. (55).

4. Results and discussion

To obtain sufficiently accurate reflected waves from solid obstacles is critical for the Brinkman penalization method for the compressible flows. Two benchmark problems are tested for the proposed method. The first one is the reflection and transmission at the interface between the fluid and the porous media of a 1-D localized acoustic pulse. This problem is used to test the proposed Brinkman penalization to check the reflected wave magnitude and phase errors. The second is the 2-D acoustic scattering by the cylinder generated by localized acoustic source. This problem was considered for the Second Computational Aeroacoustics workshop on Benchmark Problems [41]. In contrast to most of the methods used in workshop, which solved linearized Euler equations, here the full Navier–Stokes equations are solved. For the Euler equations, the benchmark problems have exact analytical solutions [42]. The full compressible Brinkman-penalized Navier–Stokes equations for acoustic Reynolds number $Re_a = 5 \times 10^5$ are solved. The time accurate DNS results for the field in computation domain are compared with analytical solutions.

4.1. Benchmark problem I: one-dimensional normal wave

The solutions for the 1-D benchmark problem are shown in Figs. 3–6. This acoustic problem is simulated in the domain $\Omega = [0, 1]$. The fluid occupies $\Omega = [0, 0.5]$, the porous media occupies $\Omega = [0.5, 1]$ and the interface

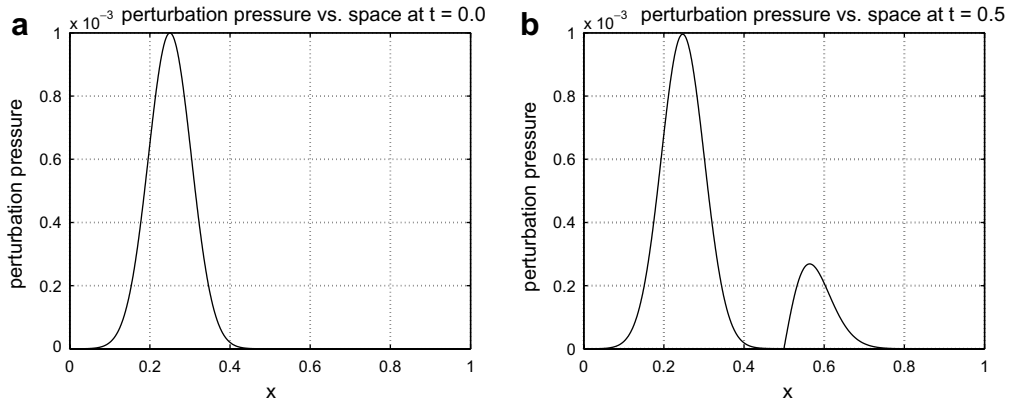


Fig. 3. 1-D problem snapshots: (a) at $t = 0.0$, (b) at $t = 0.5$ for $\phi = 10^{-3}$.

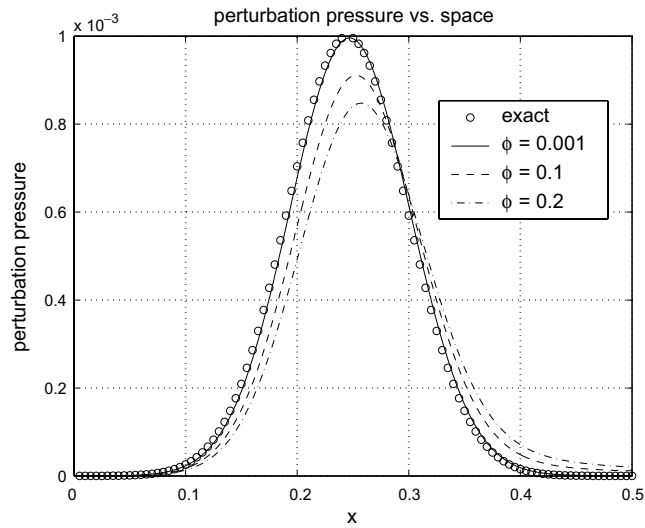


Fig. 4. 1-D problem: reflected wave comparison.

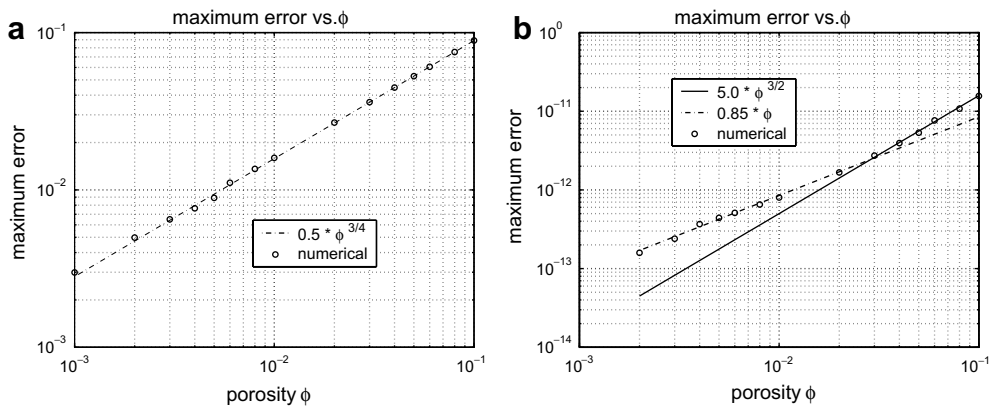


Fig. 5. 1-D problem convergence for: (a) Case 1, (b) Case 2.

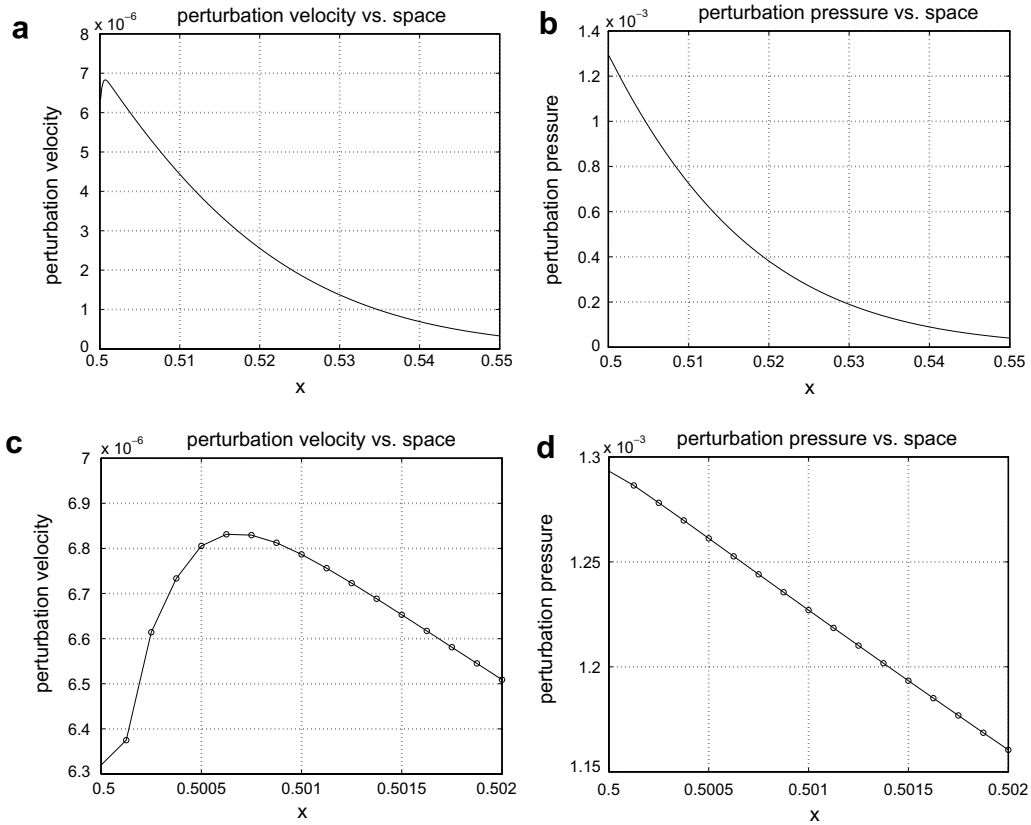


Fig. 6. Snapshots of perturbations in the porous media for: (a) velocity, (b) pressure, and in the boundary layer for: (c) velocity, (d) pressure.

is at $x = 0.5$. The initial conditions are localized density, velocity, and pressure perturbations of the Gaussian distribution:

$$\rho' = u' = p' = \epsilon \exp \left[-\ln(2) \frac{(x - 0.25)^2}{0.004} \right], \tag{80}$$

where the wave amplitude $\epsilon = 10^{-3}$, to the spatially uniform field. It represents a right-traveling acoustic wave towards the porous media. The corresponding initial conditions for the conservative variables are of the form

$$\rho = 1 + \rho', \quad m_1 = \rho u', \quad e = \frac{1}{\gamma(\gamma - 1)} + \frac{p'}{\gamma - 1} + \frac{1}{2} \rho (u')^2. \tag{81}$$

Two test cases mentioned in Section 3.4.3 are used to test the accuracy and convergence rate for the proposed method.

First, consider the problem of Case 1 in Section 3.4.3 with various porosity ϕ values, $\alpha = 10^{-2}$, $\alpha_T = 10^{-2}$, and the convergence rate of $O(\phi^{3/4})$ using the unresolved boundary layer. For efficient purpose, the space step size $\Delta x = 10^{-3}$ is used for the porosity $\phi \leq 10^{-1}$ values. Because the boundary layer thickness is less than 3×10^{-3} , there are at most 2 mesh points inside the boundary layer. Thus, the boundary layer is not resolved.

Fig. 3a shows the initial acoustic wave snapshot of the perturbation pressure. It is also the exact acoustic wave snapshot of the perturbation pressure at time $t = 0.5$ for the solid wall boundary conditions, which can be used to compare with the numerical solution for the proposed model. When the right-traveling wave hits the wall, a part of the wave is reflected back with some energy and mass losses and the rest is transmitted into the porous media. The ideal results are those with small amplitude and phase errors for the reflected wave. Note that the wave transmission happens only in the fluid part of porous media region. Fig. 3b shows a typical

acoustic wave snapshot of the perturbation pressure at time $t = 0.5$ for the porosity $\phi = 10^{-3}$. The pulse at $x = 0.25$ is the reflected acoustic wave from the wall, governed by the wave equation in the fluid region, while the wave at $x > 0.5$ is the transmitted wave, governed by the diffusion equation in the porous media region. This transmission wave in the porous media region has an obviously high amplitude. But, it occurs only in the fluid part of the porous media region. Note that the fluid occupies $\phi \ll 1$ of the total volume fraction of the porous media. Thus, this amplitude needs to be multiplied by ϕ to get the effective amplitude of the transmission wave over the whole porous media. Due to the small porosity ϕ , the actual transmission energy loss is limited and most energy is reflected back from the interface, resulting in the negligible amplitude error shown in Fig. 3a and b.

As already indicated in the error analysis section, in order for the compressible Brinkman penalization method to represent the complex geometry flows accurately, the amplitude and phase errors of the reflected waves need to be minimized. Fig. 4 is used to show the two kinds of errors for the reflected waves using the proposed method. In the figure, the exact reflected perturbation pressure from the solid wall are compared with the numerical solutions for various porosity values $\phi = 0.2$, $\phi = 0.1$, and $\phi = 10^{-3}$. It shows that the smaller the porosity, the better the amplitude and phase errors. When the porosity is sufficiently small, the numerical results are in very good agreement with the exact results. The amplitude errors are approximately 15.2%, 8.9%, and 0.3% for $\phi = 0.2$, $\phi = 0.1$, and $\phi = 10^{-3}$, respectively.

Another important aspect of the Brinkman penalization is its ability to actively control the numerical error through control parameters, ϕ , η , and η_T , by setting them to arbitrary small values. The effectiveness of the Brinkman penalization is demonstrated in Fig. 5a, where the convergence rate for the reflected waves is shown. For the numerical errors, the peak values of the reflected acoustic wave are considered. The relative error is defined as $(\epsilon - p')/\epsilon$, where $\epsilon = 10^{-3}$ is the exact wave amplitude of the pressure perturbation and p' is the numerical peak values of the pressure perturbation. The numerical results show that the errors converge in the order of $\phi^{3/4}$, which verifies the convergence rate for the unresolved boundary layer using the asymptotic analysis. The figure also shows that when the porosity is less than 5×10^{-3} , the error is less than 1%.

Next, consider the problem of Case 2 in Section 3.4.3 with various porosity ϕ values, $\alpha = \phi$, $\alpha_T = 0.4$, and the convergence rate of $O(\phi^{3/2})$ using the resolved boundary layer and $O(\phi)$ using the unresolved boundary layer. The space step size $\Delta x = 1.25 \times 10^{-4}$ is used for the porosity $\phi \leq 10^{-1}$ values. In this case, the boundary layer is resolved for larger porosity and unresolved for smaller values of ϕ . The numerical results of Case 2 are similar to the results of Case 1. For the accuracy, its results also shows that the smaller the porosity, the better the amplitude and phase errors. When the porosity is sufficiently small, the numerical results are in very good agreement with the exact results. However, the convergent rate is different from that in Case 1. Fig. 5b shows the error convergence rate for the reflected waves for Case 2. The numerical results show that the errors converge in the order of $\phi^{3/2}$ when $\phi > 2 \times 10^{-2}$ while the errors converge in the order of ϕ when $\phi < 2 \times 10^{-2}$. The difference results from whether the boundary layer is resolved or not. The results verifies the convergence rates using the asymptotic analysis. The figure also shows that when the porosity is less than 8×10^{-3} , the error is less than 1%.

Fig. 6 shows the snapshots of the velocity and pressure perturbations in the porous media and the boundary layer for $\phi = 10^{-2}$ when the incident wave hits the porous media at time $t = 0.2$. It illustrates the situation of the unresolved boundary layer. Fig. 6a and b show the perturbations in the porous media. They clearly show that the pressure perturbation is sufficiently smooth and its length scale is of $O(1)$. By contract, there is a very thin velocity boundary layer. To see the numerical approximation in the boundary layer, Fig. 6c and d show the mesh details. Because the boundary layer thickness is around 5×10^{-4} while the space step size $\Delta x = 1.25 \times 10^{-4}$, there are about only 4 mesh points in the boundary layer for the numerical simulations. It is obvious that the length scale of velocity has not been resolved. This unresolved boundary layer results in the different convergence rate, although the approach does give sufficiently accurate numerical solutions.

For this 1-D plane wave propagation problem, the wave propagation direction is always perpendicular to the wall surface and the porosity $\phi = 0.02$ gives sufficiently accurate results with the error 2.7%. For two-dimensional problems, the wave propagation direction may be oblique to the wall surface and thus part of the wave may scatter around the obstacle rather than penetrate it. In this case, the large porosity $\phi = 0.1$ may be sufficient to give accurate results.

4.2. Benchmark problem II: single source vorticity

The 2-D cylindrical acoustic benchmark problem involves a circular cylinder with radius $r = 0.5$ is located at $(4, 0)$. The initial conditions are perturbations of the Gaussian distribution:

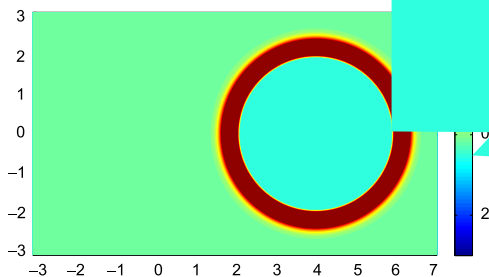
$$p' = \epsilon \exp \left[-\ln(2) \left(\frac{(x-4)^2 + y^2}{0.04} \right) \right],$$

where $\epsilon = 10^{-3}$, to the spatially uniform flow field. The initial conditions are of the form

$$\rho = 1 + p', \quad e = \frac{1}{\gamma(\gamma-1)} + \frac{p'}{\gamma-1},$$

In the problem, $\phi = 0.02$, $\alpha = 5 \times 10^{-2}$, and the numerical method used is the second-order Godunov's zonal approach [43] is used. The simulation is performed on a rectangular domain of size 10×10 . To highlight the difference among the numerical methods, the results are compared with the reference solution [43].

Due to the initial pressure perturbation, the acoustic wave propagates outwards from the cylinder. The perturbation pressure is shown at time $t = 2.0$. When the wave reflects off the right surfaces of the cylinder directly back and acoustic wave propagating towards the boundaries. The wave propagates outward. This is illustrated in Fig. 7b, a snapshot of the perturbation pressure at time $t = 2.0$. The third wave front closest to the cylinder is generated when two parts of the wave front collide and merge to the left of the surface of the cylinder. The perturbation pressure at time $t = 6.0$. The third wave surrounds the cylinder. This is illustrated in Fig. 7d, a snapshot of the perturbation pressure at time $t = 6.0$. In most parts of the domain, the three acoustic waves are separate while on some parts, the waves interact. Note that the quality of the second-order Godunov's zonal approach method for the cylinder. Fig. 7



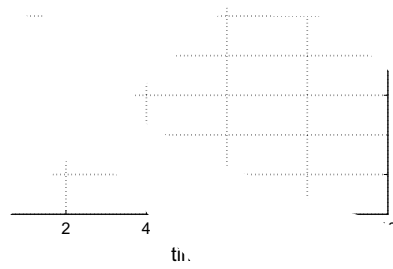
suggests physical

In order to be compared with physical points source. The points are times. All

ρ_1 observations are symmetric to the $x-E$. Note the presence of numerical results are in excellent agreement

with the analytical method can be used to catch

for compressible flows, the numerical results are compared on the computational domain of Fig. 8. The observations with respect to the circular cylinder and the time history of the perturbation pressure at five observation points that reach points A-E at different times. The numerical results are in excellent agreement with exact results for all observation points at



different directions. The proposed Brinkman penalization method gives negligible amplitude and phase errors. In contrast, the naive straightforward extension of Brinkman penalization technique [26], i.e. $\phi = 1$, results in large amplitude and phase errors, as also clearly seen in Fig. 4.

5. Conclusion

A Brinkman penalization method has been extended for numerical simulations of compressible flows around solid obstacles of complex geometries. The proposed method is based on a physically sound mathematical model for compressible flows through porous media. In addition to the penalized momentum and energy equations, the continuity equation for porous media is considered inside obstacles. In this model, the penalized porous region acts as a high impedance medium, resulting in negligible wave transmissions. The asymptotic analysis reveals that the proposed Brinkman penalization technique results in the amplitude and phase errors of order $O((\eta\phi)^{1/2})$ and $O((\eta/\eta_T)^{1/4}\phi^{3/4})$, when the boundary layer within the porous media is respectively resolved or unresolved. Thus, the amplitude and phase errors of the reflected waves can be controlled through porosity ϕ , which can be set to an arbitrary small value to guarantee the accuracy of the numerical solutions. This accuracy is crucial for aero-acoustic problems. The results of direct numerical simulation are in excellent agreement with the analytical solutions. The numerical simulations verify the accuracy and convergence rates.

The insights provided by the proposed Brinkman penalization method can be used to extend other Immersed Boundary methods to compressible flows. For example, immersed boundary implementation of the continuity equation needs to mimic the presence of high impedance media to ensure negligible wave transmission. Future work includes the generalization of the proposed Brinkman penalization for slip, rotational, and heat conducting boundary conditions, extension of the algorithm to supersonic flows with the presence of shock waves, the use of the Brinkman penalization technique with hyperbolic solvers, and the development of fully automated approach for defining complex computational domains from standard Computer Aided Design (CAD) files.

Acknowledgments

Partial support for this work was provided by the National Aeronautics and Space Administration (NASA) under Grant No. NAG-1-02116 and the National Science Foundation (NSF) under Grants No. EAR-0242591, EAR-0327269 and ACI-0242457. This support is gratefully acknowledged.

References

- [1] J.F. Thompson, Z.U.A. Warsi, C.W. Mastin, Boundary fitted coordinate systems for numerical solution of partial differential equations – a review, *J. Comput. Phys.* 47 (1982) 1–108.
- [2] D.J. Mavriplis, Accurate multigrid solution of the euler equations on unstructured and adaptive meshes, *AIAA J.* 28 (1990) 213–221.
- [3] C.S. Peskin, The immersed boundary method, *Acta Numer.* (2002) 479–517.
- [4] R. Mittal, G. Iaccarino, Immersed boundary methods, *Annu. Rev. Fluid Mech.* 37 (2005) 239–261.
- [5] C.S. Peskin, Flow patterns around heart valves: a digital computer method for solving the equations of motion, Ph.D. Thesis, Albert Einstein College of Medicine, 1972.
- [6] M.C. Lai, C.S. Peskin, An immersed boundary method with formal second order accuracy and reduced numerical viscosity, *J. Comput. Phys.* 160 (2000) 705–719.
- [7] D. Goldstein, R. Handler, L. Sirovich, Modeling a no-slip flow boundary with an external force field, *J. Comput. Phys.* 105 (1993) 354–366.
- [8] E.M. Saiki, S. Biringen, Numerical simulation of a cylinder in uniform flow: application of a virtual boundary method, *J. Comput. Phys.* 123 (1996) 450–465.
- [9] J.W. Purvis, J.E. Burkhalter, Prediction of critical mach number for store configurations, *AIAA J.* 17 (11) (1979) 1170–1177.
- [10] D.K. Clarke, M.D. Salas, H.A. Hassen, Euler calculations for multielement airfoils using cartesian grids, *AIAA J.* 24 (3) (1986) 353–358.
- [11] D.D. Zeeuw, K.G. Powell, An adaptively refined cartesian mesh solver for the euler equations, *J. Comput. Phys.* 104 (1993) 56–68.
- [12] M.J. Berger, M.J. Aftosmis, Aspects (and aspect ratios) of cartesian mesh methods, in: Proceedings of the 16th International Conference on Numerical Methods Fluid Dynamics.
- [13] Y.H. Tseng, J.H. Ferziger, A ghost-cell immersed boundary method for flow in complex geometry, *J. Comput. Phys.* 192 (2003) 593–623.

- [14] E. Arquis, J.P. Caltagirone, Sur les conditions hydrodynamiques au voisinage d'une interface milieu fluide – milieu poreux: application à la convection naturelle, *C.R. Acad. Sci. Paris II* 299 (1984) 1–4.
- [15] P. Angot, C.-H. Bruneau, P. Fabrie, A penalization method to take into account obstacles in viscous flows, *Numerische Mathematik* 81 (1999) 497–520.
- [16] P. Angot, Analysis of singular perturbations on the brinkman problem for fictitious domain models of viscous flows, *Math. Meth. Appl. Sci.* 22 (1999) 1395–1412.
- [17] R. Ghias, R. Mittal, T.S. Lund, A non-body conformal grid method for simulation of compressible flows with complex immersed boundaries, *AIAA Paper No. 2004-0080*.
- [18] C. Chung, Wave propagation and scattering in computational aeroacoustics, Ph.D. dissertation, Department of Aerospace Engineering, Pennsylvania State University, University Park, PA, 1995.
- [19] C. Chung, P.J. Morris, Acoustic scattering from two- and three-dimensional bodies, *J. Comput. Acoust.* 6 (1998) 357–375.
- [20] O.A. Laik, P.J. Morris, Direct simulation of acoustic scattering by two- and three-dimensional bodies, *J. Aircraft* 37 (2000) 68–75.
- [21] A. Agarwal, P.J. Morris, Direct simulation of acoustic scattering by a rotorcraft fuselage, *AIAA Paper No. 2000-2030*.
- [22] R. Cohen, A. Ooi, G. Iaccarone, Towards the application of the impedance mismatch method to the expansion about incompressible flow acoustic equations, in: *Proceedings of the Summer Program 2006*, Center for Turbulence Research.
- [23] N.K.-R. Kevlahan, O.V. Vasilyev, An adaptive wavelet collocation method for fluid-structure interaction at high Reynolds numbers, *SIAM J. Sci. Comput.* 26 (6) (2005) 1894–1915.
- [24] O.V. Vasilyev, C. Bowman, Second generation wavelet collocation method for the solution of partial differential equations, *J. Comp. Phys.* 165 (2000) 660–693.
- [25] O.V. Vasilyev, Solving multi-dimensional evolution problems with localized structures using second generation wavelets, *Int. J. Comp. Fluid Dyn.* 17 (2) (2003) 151–168, Special issue on High-resolution methods in Computational Fluid Dynamics.
- [26] Q. Liu, O.V. Vasilyev, Hybrid adaptive wavelet collocation–Brinkman penalization method for unsteady RANS simulations of compressible flow around bluff bodies, *AIAA Paper No. 2006-3206*.
- [27] W.S. Edwards, L.S. Tuckerman, R.A. Friesner, D.C. Sorensen, Krylov methods for the incompressible Navier–Stokes equations, *J. Comp. Phys.* 110 (1994) 82–102.
- [28] D.A. Nield, A. Bejan, *Convection in Porous Media*, second ed., Springer, 1999.
- [29] O.M. Phillips, *Flow and Reactions in Permeable Rocks*, Cambridge University Press, 1991.
- [30] M. Kaviany, *Principles of Heat Transfer in Porous Media*, Springer-Verlag, 1991.
- [31] H.P.G. Darcy, *Les fontaines publiques de la ville de dijon*, Victor Dalmont, Paris, 1856.
- [32] H.C. Brinkman, A calculation of the viscous force exerted by a flowing fluid on a dense swarm of particles, *Appl. Sci. Res. A1* (1947) 27–34.
- [33] H.C. Brinkman, On the permeability of media consisting of closely packed porous particles, *Appl. Sci. Res. A1* (1947) 81–86.
- [34] R.A. Wooding, Steady state free thermal convection of liquid in a saturated permeable medium, *J. Fluid Mech.* 2 (1957) 273–285.
- [35] K. Vafai, C.L. Tien, Boundary and inertia effects on flow and heat transfer in porous media, *Int. J. Heat Mass Transfer* 24 (1981) 195–203.
- [36] C.T. Hsu, P. Cheng, Thermal dispersion in a porous medium, *Int. J. Heat Mass Transfer* 33 (1990) 1587–1597.
- [37] J.L. Beck, Convection in a box of porous material saturated with fluid, *Phys. Fluids* 15 (1972) 1377–1383.
- [38] D.T. Blackstock, *Fundamentals of Physical Acoustics*, Wiley, 2000.
- [39] C. Laney, *Computational Gasdynamics*, Cambridge University Press, 1998.
- [40] M.D. Greenberg, *Advanced Engineering Mathematics*, Prentice Hall, Inc., 1998.
- [41] C.K.W. Tam, J.C. Hardin (Eds.), *Second Computational Aeroacoustics (CAA) Workshop on Benchmark Problems*, NASA Conference Publication 3352, 1997.
- [42] C.K.W. Tam, Derivation of an exact solution for the scattering of an acoustic pulse by a circular cylinder, Private communication.
- [43] J.B. Freund, Proposed inflow/outflow boundary condition for direct computation of aerodynamic sound, *AIAA J.* 35 (1997) 740–742.